IOP Publishing Eur. J. Phys. 47 (2026) 035801 https://doi.org/10.1088/1361-6404/ae5bd4

European Journal of Physics

PAPER

RECEIVED
16 September 2025

REVISED
23 March 2026

ACCEPTED FOR PUBLICATION
6 April 2026

PUBLISHED
18 May 2026

Front-face magnetic induction of a cylindrical neodymium magnet stack:exact telescoping model and effective exponential approximation

Čeněk Kodejška *

Department of Math and Physics, PSJG, Hradec Králové, Czech Republic

* Author to whom any correspondence should be addressed.

E-mail: cenek.kodejska@seznam.cz

Keywords: magnetic field, neodymium magnets, terminal velocity, educational experiment, eddy curents, exponential approximation

Supplementary material for this article is available online

Abstract

We present a combined theoretical and experimental study of the magnetic field of cylindrical stacks of identical neodymium magnets. Starting from the standard expression for the axial magnetic induction of a uniformly magnetized cylinder, we derive an approximate analytical expression for the radial component based on Maxwell's equation $\nabla B = 0$. The magnetic induction at the front face of the stack is shown to be expressible as a telescoping sum of individual magnet contributions, yielding a compact closed-form expression. Over experimentally accessible ranges of stack height, the discrete dependence of the front-face induction on the number of magnets can be accurately approximated by an exponential saturation law equivalent to a geometric-series representation. The relative deviation between the exact magnetostatic model and the exponential approximation remains below 5% within measurement uncertainty for the geometries investigated. Finally, we demonstrate how this field model provides physical insight into the dependence of terminal velocity on stack length for magnets falling through conducting tubes. The approach is well suited for undergraduate teaching and advanced secondary-school laboratory work.

1. Introduction

Analytical descriptions of the magnetic field of permanent magnets remain important both for applications and for teaching, because they connect measurable quantities (field profiles, forces, moments) with compact magnetostatic models. For axially magnetized cylindrical magnets, Song and Shuai [1] proposed an analytical field model that explicitly includes demagnetization effects, aiming at improved realism for finite-size Nd–Fe–B magnets. In a complementary educational context, Martín-Luna *et al* [2] presented a careful magnetostatic treatment of the scalar potential and magnetic field of a cylindrical magnet, emphasising closed-form expressions and derivations suitable for students. Related methodology based on integral formulations for the magnetic field intensity of a cylindrical permanent magnet was discussed by Cava *et al* [3], who focused on practical evaluation of the field from magnet geometry.

Several works address either more complex geometries or the validity of common approximations. Zhang *et al* [4] analysed spatial magnetic-field distributions produced by periodically arranged permanent-magnet rolls in a circumferential–axial arrangement, motivated by engineering and process applications. Adams [5] studied 'tractor magnet' configurations in two dimensions and combined theory with realizations to illustrate non-trivial field shaping. Shulman [6] examined the magnetic field of a cylindrical permanent magnet with emphasis on comparing experimentally obtained field data with analytical models (including widely used idealised representations) and on clarifying their range of validity. Magnetic-field penetration and boundary effects in the presence of high-permeability screening materials were treated by Erofeenko [7] through an axially symmetric mathematical model of field transmission through a plane permalloy screen.

A closely related pedagogical line concerns eddy-current braking when a magnet falls through a conducting tube. The classic quantitative treatment of this demonstration was given by MacLatchy *et al* [8]. Levin *et al* [9] provided a pedagogical model of eddy currents and magnetic damping, while Roy [10] presented a dimensional-analysis approach. Experimental and modelling refinements for the falling-magnet experiment include the use of the setup to measure electrical conductivity (Íñiguez and Raposo [11]), laboratory-oriented investigations of magnet motion and magnetic braking (Ireson and Twidle [12]), and extended modelling of the damping force and configurations such as magnets falling near the pipe wall or in pairs (Donoso *et al* [13]). The influence of pipe-wall thickness on the retarding drag has been investigated in an educational setting by Maryam *et al* [14].

A recent contribution directly linking the falling-magnet experiment with parameter determination is the work of Pal *et al* [15], who analysed the motion of a permanent magnet falling through a conducting pipe with the explicit aim of determining its magnetic dipole moment from measured terminal velocity. Their work combines accessible measurements with a simplified eddy-current model, showing how the classic demonstration can be used for quantitative parameter extraction in teaching laboratories.

Independent of the tube experiment, several papers focus on extracting magnet parameters from simple measurements. Camacho and Sosa [16] developed an approach for calculating the magnetic field of azimuthally symmetric permanent magnets and discussed practical evaluation of magnet parameters. Connors [17] presented an instructional study of the magnetic field of disk magnets, combining direct measurements with simple analytical modelling. By comparing measured axial field profiles with theoretical expressions for uniformly magnetized cylinders, the work illustrates how basic laboratory data can be used to test magnetostatic formulas and estimate effective magnet parameters.

In a different educational design, Médjahdi [18] proposed determining the magnetization of a permanent magnet from a static-equilibrium experiment in which an external field is tuned by adding or removing magnets from a stack. Such work highlights how changing the number of magnets in a stack provides a controlled way to vary the magnetic field in accessible laboratory conditions. For reference and notation, we follow standard magnetostatics conventions as presented in textbooks such as Griffiths [19].

Despite this broad literature, the specific question of how the *front-face magnetic induction of a stack of identical cylindrical magnets* depends on the number of magnets is rarely treated in a way that is both analytically transparent and experimentally convenient for teaching laboratories. In particular, while single-cylinder expressions are standard, a compact interpretation of the *discrete saturation behaviour* with increasing stack length can be valuable for students who are simultaneously learning superposition ideas and simple series models. The present work addresses this by (i) expressing the front-face field of a stack as a telescoping sum of contributions from successive magnets, yielding a closed-form dependence on stack length, and (ii) introducing an effective exponential (geometric-series) approximation that captures the observed saturation trend over experimentally relevant ranges. We then connect this field scaling to the qualitative behaviour of terminal velocity in the conducting-tube demonstration.

The aim of the present paper is twofold:

1. To derive a compact expression for the radial component of magnetic induction near the axis of a cylindrical magnet stack and to express the front-face induction as a telescoping sum of contributions from individual magnets.
2. To show that, over experimentally accessible ranges, the discrete behaviour of the front-face induction can be approximated by an exponential saturation law equivalent to a geometric-series representation, which provides a useful pedagogical model.

We further demonstrate how this description helps to interpret the observed dependence of terminal velocity on stack height.

2. Theoretical background

2.1. Axial magnetic induction

To derive an expression for the radial component of the magnetic field of a cylindrical stack of magnets, we begin with the well-known relation for the axial component of magnetic induction along the axis of the stack. This expression has been presented or directly derived in [19]. For convenience, it may be written in the following form:

$$B_z(z) = \frac{B_{\text{rem}}}{2}\left(\frac{z + h/2}{\sqrt{(z + h/2)^2 + r_m^2}} - \frac{z - h/2}{\sqrt{(z - h/2)^2 + r_m^2}}\right), \tag{1}$$

where B_{rem} denotes the remanent induction of the magnet or the stack, h is the total height of the stack composed of n elementary magnets, each of height d and radius r_m, and z is the axial coordinate measured from the origin placed at the centre of the elementary magnet (or of the entire stack).

2.2. Radial component of magnetic induction derived from the axial field

From the standard expression (1) for the axial component of magnetic induction of a uniformly magnetized cylinder of height h and radius $r_m = D/2$, we obtain an approximate expression for the radial component by using Maxwell's equation $\nabla \cdot \mathbf{B} = 0$. In cylindrical coordinates, expanded about $r = 0$ gives, to first order in r, $B_r(r,\ z) \approx -\frac{r}{2}\frac{\partial B_z(0,\ z)}{\partial z}$. Differentiating equation (1) then yields the compact analytical form

$$B_r(z) = \frac{B_{\text{rem}}}{2}\left(\frac{1}{\left[1 + \left(\frac{2z - h}{2r_m}\right)^2\right]^{\frac{3}{2}}} - \frac{1}{\left[1 + \left(\frac{2z + h}{2r_m}\right)^2\right]^{\frac{3}{2}}}\right). \tag{2}$$

In the front-face measurements, the probe was positioned at a fixed radial offset $r \approx r_m$ (section 5). Although the derivation strictly applies near the axis, we use equation (2) here as an effective analytical model for the front-face peak; its adequacy is supported by the agreement with the measured maxima within the ≈5% instrumental uncertainty (section 5).

3. Mathematical model based on exponential (geometric-series) approximation

3.1. Front-face induction and telescoping sum

As shown in the experimental section, the local maximum of the radial component, i.e. the maximum value of B_r occurs close to the front face of the stack, corresponding to the condition $z \approx h/2$. Evaluating the radial component at the front face of a stack of n identical magnets (total height $h = nd$) yields

$$B_r(n) \approx \frac{B_{\text{rem}}}{2}\left(1 - \frac{1}{[1 + (nd/r_m)^2]^{3/2}}\right) = \frac{B_{\text{rem}}}{2}\left(1 - \frac{1}{[1 + (n/k)^2]^{3/2}}\right), \tag{3}$$

where $k = r_m/d$.

Experimentally, the peak of $B_r(z)$ occurs within $\Delta z \lesssim (0.1\text{–}0.2)d$ of the front face for the geometries studied; we therefore evaluate the model at $z = h/2$ for a compact closed-form dependence on n.

Alternatively, by considering the contribution of each individual magnet at distances $z_n = (2n - 1)d/2$, the front-face induction can be written as

$$B_r(n) = \sum_{i=1}^{n} \Delta_i, \tag{4}$$

where each term corresponds to the difference between two successive inverse-power expressions. The resulting sum is telescoping and reduces exactly to equation (3). This representation provides a transparent physical interpretation: the field at the front face is formed by the cumulative contributions of individual magnets at increasing distances.

3.2. Exponential approximation

Equation (3) describes a monotonic saturation towards $B_\infty = \lim_{n\to\infty} B_r(n) = \frac{B_{\text{rem}}}{2}$.

Consequently, it is convenient to introduce the *saturation deficit* $\Delta_n = B_\infty - B_r(n)$, which quantifies how far the stack is from the saturated front-face induction.

Over a finite experimental range of n (typically $n \leqslant 10 - 20$ in our measurements), the discrete sequence $B_r(n)$ is well approximated by an exponential saturation law, i.e. by a geometric sequence for the deficit Δ_n:

$$\Delta_n = \Delta_1 r^{n-1}, \quad 0 < r < 1, \tag{5a}$$

or, equivalently,

$$B_r(n) = B_\infty - (B_\infty - B_r(1))r^{n-1}. \tag{5b}$$

This exponential law can be rewritten in a form suggestive of a geometric series. Using $B_\infty = B_r(1)/(1 - r)$ as an effective fitted limit, equation (5*b*) becomes

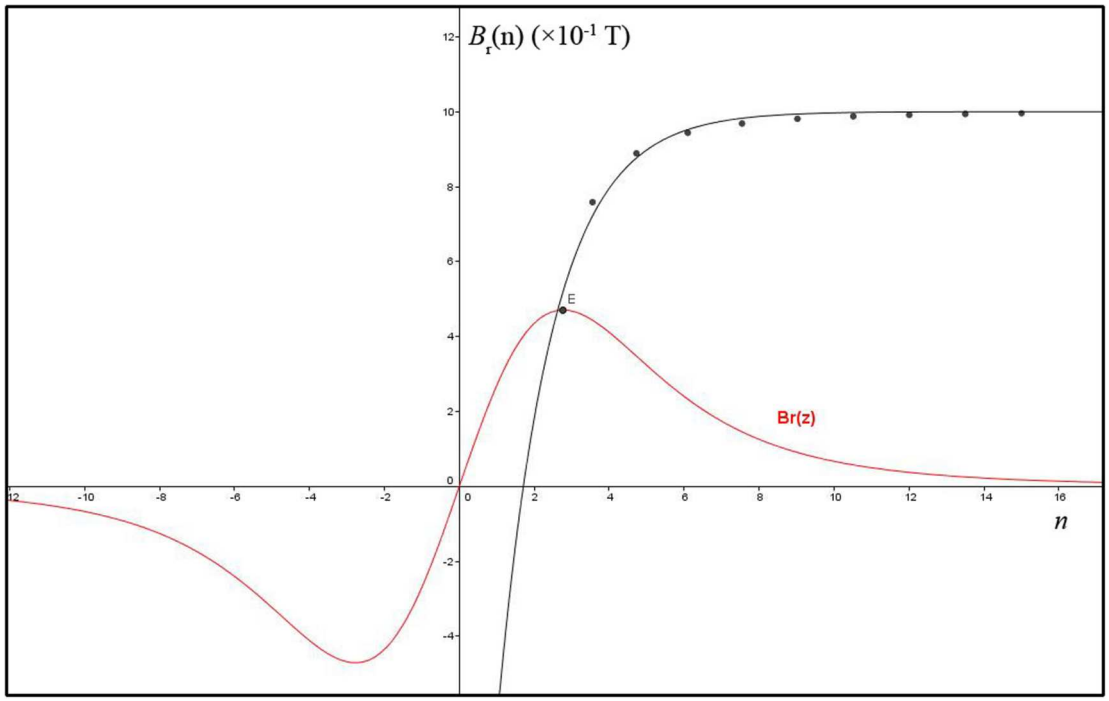

Figure 1. The maxima predicted by equation (3) (discrete points) together with the geometric-series saturating curve (5*c*) depending on number of magnets n in a stack.

$$B_r(n) = B_r(1)(1 + r + r^2 + \ldots + r^{n-1}) = B_r(1)\frac{1 - r^n}{1 - r}, \tag{5c}$$

where the common ratio r is treated as an effective parameter determined from experimental data. In this interpretation, equation (5*c*) is not claimed to be an exact identity following from magnetostatics; rather, it provides a compact approximation of the experimentally observed exponential saturation law $B_r(n) \approx B_\infty(1 - r^n)$ over the experimental range.

In the geometric approximation, the limiting value B_∞ is related to the fitted parameter r and the measured value $B_r(1)$ through $B_\infty = B_r(1)/(1 - r)$, which serves as an effective experimental parameter rather than a strict magnetostatic identity.

Figure 1 illustrates this idea: the values calculated from equation (3) (discrete points) follow a saturating trend which can be represented, within experimental uncertainty, by the continuous geometric-series curve (5*c*) over the measured range of n.

For the geometries investigated in our experimental work, the relative deviation between equation (3) and the exponential approximation (5*c*) remains below 5% within measurement uncertainty.

3.3. Dependence of the effective ratio on magnet aspect ratio

The fitted effective ratio r depends primarily on the aspect ratio of the elementary magnet. In our data, this dependence is well captured by an empirical exponential function of $x = d/D$,

namely

$$r(x) = r_0 e^{-\gamma x}, \tag{6}$$

with constants r_0, γ obtained from the fit (see figure 3). This compact parameterization provides a convenient way to compare different magnet sets and to build a simple predictive model for educational laboratory work. The fitted parameter $r(x)$ depends primarily on the aspect ratio d/D of the elementary magnet and follows approximately an exponential dependence on this ratio.

We found from experimental values presented in table 1 that the fitted parameter $r(x)$ depends approximately exponentially on $x = d/D$: $r(x) = 1.115\ e^{-2.53x}$. Figure 2 shows the linearized dependence $\ln(r(x)) = 0.109 - 2.53x$, obtained by plotting $r(x)$ on a logarithmic scale.

$B_z(0)$—calculated value of axial induction in the magnet axis for $z = 0$ m and $h = nd$ according to equation (1)

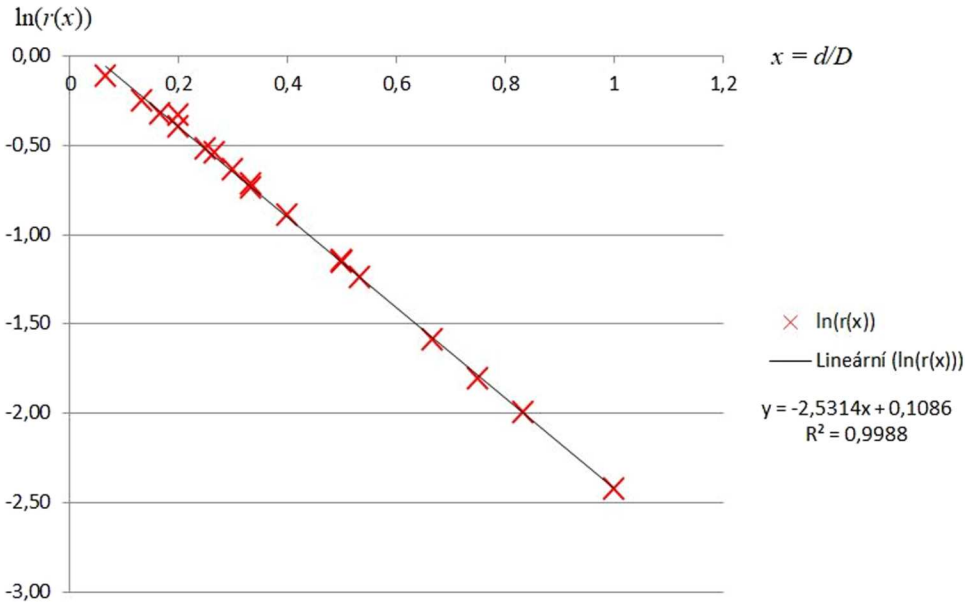

Figure 2. Linear dependence of $\ln(r(x))$ on the ratio $x = d/D$ according to equation (6).

Table 1. Parameters of neodymium magnets N38 and N42.

D (mm)	d (mm)	$x = d/D$	$n_{\max}$	$B_z(0)$ (T)	$B_z\left(\frac{h}{2}\right)/B_r\left(\frac{h}{2}\right)$ (T)	Type	$r(x)$
8	2	0.25	10	1.15	0.442/0.325	N38	0.59
8	4	0.50	10	1.27	0.459/0.325	N42	0.31
8	6	0.75	10	1.23	0.457/0.325	N38	0.16
10	2	0.20	20	1.26	0.447/0.373	N42	0.71
10	3	0.30	20	1.28	0.487/0.383	N42	0.53
10	4	0.40	10	1.20	0.481/0.378	N38	0.41
10	5	0.50	10	1.25	0.482/0.371	N38	0.31
10	10	1.00	6	1.31	0.489/0.395	N42	0.09
12	2	0.17	20	1.25	0.473/0.387	N42	0.72
12	4	0.33	10	1.25	0.490/0.408	N42	0.49
12	6	0.50	10	1.27	0.490/0.401	N42	0.32
12	8	0.67	10	1.29	0.493/0.408	N42	0.20
12	10	0.83	10	1.23	0.493/0.408	N38	0.14
15	1	0.07	20	0.99	0.460/0.413	N38	0.89
15	2	0.13	20	1.16	0.491/0.442	N38	0.78
15	3	0.20	20	1.20	0.499/0.447	N38	0.67
15	4	0.27	10	1.16	0.489/0.449	N38	0.58
15	5	0.33	10	1.19	0.496/0.460	N38	0.48
15	8	0.53	10	1.28	0.548/0.495	N42	0.29

$B_z\left(\frac{h}{2}\right)$, $B_r\left(\frac{h}{2}\right)$—experimentally measured values of axial and radial induction at the front of the stack

$$B_{\mathrm{rem}}(N38) = 1.24(2)\ \mathrm{T},\quad B_{\mathrm{rem}}(N42) = 1.30(2)\mathrm{T}.$$

Table 1 above provides an overview of the magnet sets used and their parameters, as well as the measured axial and radial magnetic induction values at the front of the stack and the fitted value of the quotient $r(x)$ in equation (5c).

According to equation (1), the value $B_z(0)$ corresponds to the maximum of the axial magnetic induction function, which corresponds to the centre of the stack $(z = 0)$.

4. Theoretical derivation of the expression for the ratio of the radial component in a magnet stack

Now, let us consider the distance from the front of the stack to the centre of individual magnets in the stack, assuming the height of one magnet is d. For the first magnet, $z = \frac{1}{2}d$; for two magnets, $z = \frac{3}{2}d$, and so on. Generalizing this, we arrive at the relationship $z(n) = (2n - 1)\frac{d}{2}$. Substituting these values into equation (2) one by one yields the sequence of individual values $B_r(n)$:

$$B_r(n) = \frac{B_{\text{rem}}}{2}\left(\frac{1}{\left[1 + \left(\frac{(n-1)d}{r_m}\right)^2\right]^{3/2}} - \frac{1}{\left[1 + \left(\frac{nd}{r_m}\right)^2\right]^{3/2}}\right). \tag{7}$$

The successive sums of which should correspond to equation (3), representing the maximum induction values at the front of the stack. Equation (5c) performs the same task mathematically, using the sum formula for geometric series.

Adding up the individual values $B_r(n)$ sequentially allows us to find a general expression for the sum function $s_n(k)$:

$$s_n(k) = \frac{B_{\text{rem}}}{2}\left(1 - \frac{1}{[1 + (nd/r_m)^2]^{3/2}}\right) = \frac{B_{\text{rem}}}{2}\left(1 - \frac{1}{[1 + (n/k)^2]^{3/2}}\right), \tag{8}$$

where $k = \frac{r_m}{d}$. Equation (8) is identical to equation (3), which was derived differently. Thus, the front-face induction can be written as a telescoping sum of contributions from successive magnets. Over the measured range, the resulting discrete values can be approximated by a geometric-series (exponential) saturation model.

In a similar way, the following expression (9) can be found for the quotient $q(k)$ of the geometric sequence given by equation (8):

$$q_n(k) = \frac{B_r(n+1)}{B_r(n)} = \frac{\frac{1}{\left[1 + \left(\frac{n}{k}\right)^2\right]^{\frac{3}{2}}} - \frac{1}{\left[1 + \left(\frac{n+1}{k}\right)^2\right]^{\frac{3}{2}}}}{\frac{1}{\left[1 + \left(\frac{n-1}{k}\right)^2\right]^{\frac{3}{2}}} - \frac{1}{\left[1 + \left(\frac{n}{k}\right)^2\right]^{\frac{3}{2}}}}. \tag{9}$$

The exact ratio $q_n(k)$ is dependent on the number n of magnets in the stack and the inverse ratio $r_n(k) = 1/q_n(k)$ is the theoretical limit for effective fit parameter $r(x)$ given by equation (6).

5. Experimental measurement of magnetic induction

The values B_z and B_r in the sixth column of table 1 are the experimentally measured axial and radial values at the front of the magnet set for a given number n of magnets, measured using a Voltcraft GM-70 teslameter with two ranges: 300 mT × 0.01 mT and 3000 mT × 0.1 mT, with a measurement error of 5% for both. The teslameter can also record the maximum and minimum measured values, which was particularly useful when measuring the radial component of the induction. This made it possible to measure magnetic induction in a school laboratory environment with sufficient accuracy. As mentioned in the conclusion of the experimental section, this teslameter can be used to conduct simple laboratory exercises with students to measure the basic parameters of neodymium magnets.

For each set of magnets listed in table 1, we measured the magnetic induction values in the axial and radial directions for each n in the range $(1;\ n_{\max})$ using the teslameter. As this is a large amount of data, the following graphs and tables only show data representative of all types of elementary magnet (flat, medium and high), without compromising generality. The conclusions drawn from our measurements apply to all sets in table 1. The dataset is publicly available at [20].

The experimentally measured maximum values of the $B_r(z = h/2)$ function for selected sets are presented in figures 3–4 as red crosses. The green squares show the theoretical values calculated using equation (3) for the radial component of magnetic induction, with a 5% error bar, according to our proposed function. For radial measurements, the probe was positioned at $r = r_m$ relative to the magnet axis.

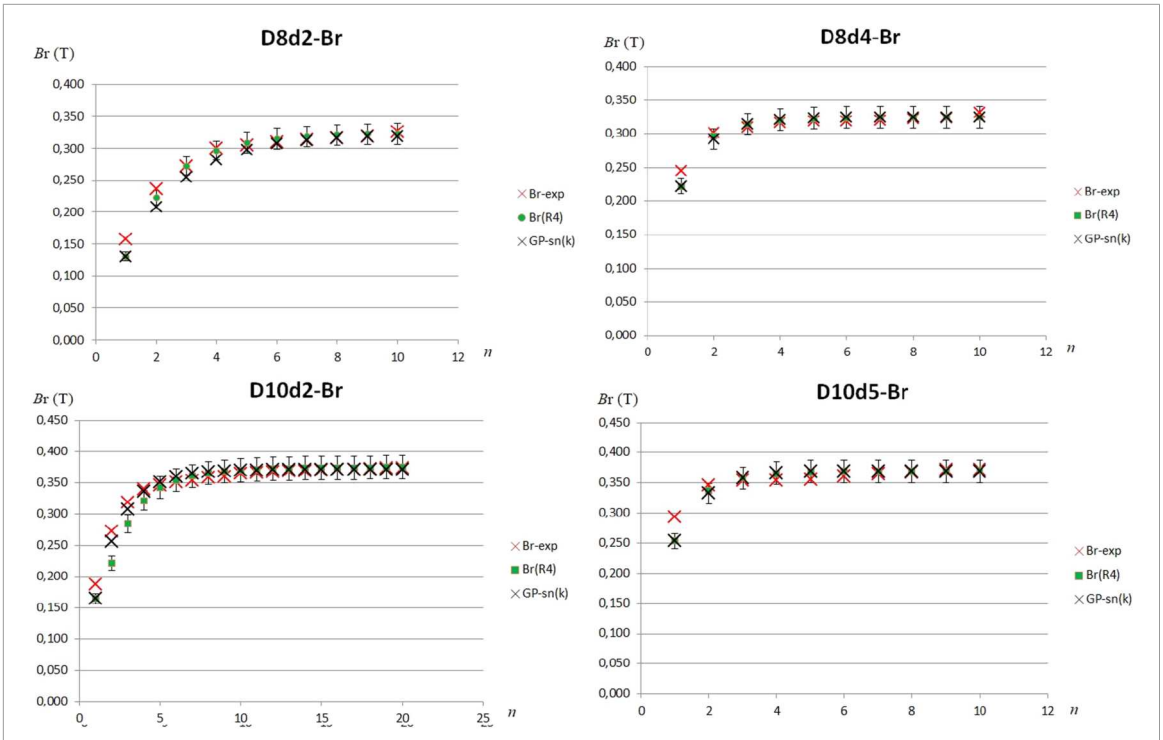

Figure 3. Graphs showing the radial component of induction for the magnet sets D8d2, D8d4, D10d2 and D10d5.

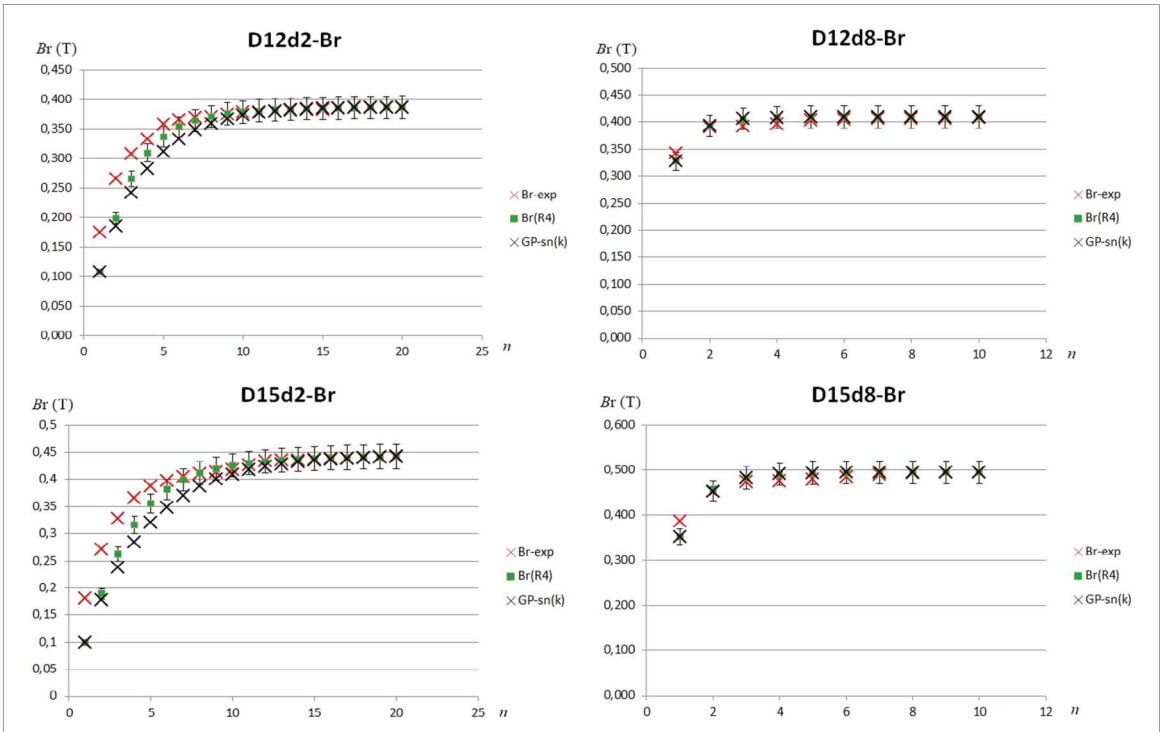

Figure 4. Graphs showing the radial component of induction for the magnet sets D12d2, D12d8, D15d2, and D15d8.

The mathematical approximation using the equation (8) is shown by the black crosses. For simplicity, the same value of $r\,(x)$ was used for the given set in the calculation, as shown in the last column of table 1.

Several conclusions can be drawn from all the graphs in figures 3–4. For small values $d < r_m$, i.e. for flat magnets, the radial component B_r is as dominant as the axial component B_z and the measured values deviate more from the theoretical models given by equations (3) or (8), approaching the values according to equation (1). The magnetic field of flat magnets 'spreads' more to the sides.

When the magnet's height reaches $d \cong r_m$, the cylindrical shape of the stack and the axial component of induction begin to dominate. The radial induction values then agree with the theoretical calculations, with a relative deviation less than 5%.

When $d > r_m$ and the magnetic field of the entire set is rapidly saturated, the agreement between the experimental and theoretical data is less than 2%.

The graphs also demonstrate a very good correlation between the theoretical calculation of the radial component B_r according to equation (3) and the mathematical model expressed by the equation (8). In most cases, the relative deviation between the values of the two theoretical models is also less than 5%. In our opinion, this supports the usefulness of a geometric-series approximation over finite ranges of n. The first term of this series is the magnetic induction value of an elementary magnet, which must, however, always be determined experimentally.

6. Terminal velocity of a magnet stack in a conducting tube

6.1. Magnetic braking force and terminal velocity

When a magnet stack moves with velocity v inside a conducting tube, eddy currents are induced in the tube walls. The interaction between these currents and the magnetic field of the magnet produces a retarding force that opposes the motion.

Following standard pedagogical treatments of eddy-current braking in this experiment [8–12, 17], we model the tube as a stack of thin conducting rings. Then the magnetic braking force may be derived from the Lorentz force acting on the induced currents. For an elementary ring of radius R and height $\mathrm{d}z$, the induced electromotive force is $\mathcal{E} = B_r L v$, where $L = 2\pi R$ is the ring circumference and B_r is the radial component of the magnetic induction at the tube wall.

The induced current is $I = \mathcal{E}/R_{\mathrm{el}}$ with the electrical resistance R_{el} of the elementary ring. Using Ohm's law and the conductivity σ, the differential magnetic force acting on the ring can be written in the form

$$\mathrm{d}F = 2\pi R v \sigma B_r^2 \, \mathrm{d}z \, \mathrm{d}R. \tag{10}$$

This expression shows explicitly that the braking force is proportional to v and to B_r^2, a key point for the subsequent analysis.

6.2. Dipole approximation for the radial field

For analytical tractability, and in accordance with previous studies [8, 9, 17], we approximate the magnetic field of the stack at the tube wall by that of an effective magnetic dipole with moment m_B

$$B_r(z) = \frac{3\mu_0 m_B}{4\pi} \frac{zR}{(R^2 + z^2)^{5/2}}. \tag{11}$$

This approximation is valid when the tube radius exceeds the characteristic size of the magnet and when the dominant contribution to the braking force arises from distances comparable to the tube radius. In practice this requires $R \gtrsim r_m$ and tube lengths large compared to the magnet so that end effects are negligible.

Substituting equation (11) into (10) and integrating over the tube wall yields

$$F_m = \int \mathrm{d}F = \left(\frac{3\mu_0 m_B}{4\pi}\right)^2 2\pi v\sigma \int_{R_i}^{R_o} \int_{-\infty}^{\infty} R^3 \frac{z^2}{(R^2 + z^2)^5} \mathrm{d}z\mathrm{d}R \, . \tag{12}$$

This double integral can be evaluated analytically, yielding

$$\int_{R_i}^{R_o} \int_{-\infty}^{\infty} R^3 \frac{z^2}{(R^2 + z^2)^5} \mathrm{d}z\mathrm{d}R = \frac{5\pi}{384}\left(\frac{1}{R_i^3} - \frac{1}{R_o^3}\right). \tag{13}$$

Final form for F_m after substituting equation (13) to (12) is then

$$F_m = \frac{45}{3072} v\sigma (\mu_0 m_B)^2 \left(\frac{1}{R_i^3} - \frac{1}{R_o^3}\right). \tag{14}$$

The proportionality $F_m \propto v$ confirms that a terminal velocity is reached when $mg = F_m$. Solving for the terminal velocity gives

$$v_t = \frac{3072}{45} \frac{mg}{(\mu_0 m_B)^2 \sigma w} \frac{(R_i R_o)^3}{(R_i^2 + R_i R_o + R_o^2)}. \tag{15}$$

For completeness, we should mention that in equation (15), m represents the total weight of the stack, σ is the conductivity of the tube material, w is the thickness of the tube wall, and R_i and R_o are the inner and outer radii of the tube, respectively.

In the thin-wall limit of $R_i \approx R_o = R$, this reduces to the well-known MacLatchy expression [8],

$$v_t = \frac{1024}{45}\frac{mg}{(\mu_0 m_B)^2}\frac{R^4}{\sigma w}. \tag{16}$$

6.3. Dependence on stack height

The key quantity controlling the braking force is the magnetic moment m_B, which scales linearly with n under the assumption of negligible demagnetization interaction between magnets in direct contact. This linear scaling corresponds to treating the stack as a uniformly magnetized body of volume proportional to n.

However, the previous section shows that the *radial magnetic induction at the tube wall does not grow linearly with* n but exhibits saturation behaviour. The saturation of $B_r(n)$ does not contradict this linear scaling, since it reflects geometric field redistribution rather than reduction of total dipole moment. Since the braking force scales approximately with B_r^2, the saturation of $B_r(n)$ naturally leads to a non-monotonic dependence of $v_t(n)$.

Using the exponential approximation $B_r(n) \approx B_\infty(1 - r^n)$, one obtains, at a qualitative level,

$$v_t(n) \propto \frac{n}{B_r(n)^2} \approx \frac{n}{B_\infty^2(1 - r^n)^2}. \tag{17}$$

This expression captures the experimentally observed features: for small n, B_r increases rapidly and v_t decreases; beyond a characteristic value n_0, the growth of B_r slows down; the function may exhibit a shallow minimum before increasing again.

Equation (17) is intended as a scaling argument; quantitative predictions use equations (15)–(16) together with measured $B_r(n)$.

6.4. Empirical correction factors

In real experiments, additional effects influence the terminal velocity:

1. Finite tube thickness.
2. Deviation from the ideal dipole field.
3. Possible tilt of the magnet axis relative to the tube axis.
4. Air friction due to the cavity between the magnet and the tube wall.

Rather than incorporating these effects into a full electromagnetic boundary-value problem, we introduce a single geometry-dependent correction factor $\eta(n) \approx 1$ for the geometries investigated that accounts for deviations from the ideal dipole model:

$$v_t^{(\mathrm{exp})} = v_t^{(\mathrm{ideal})}\eta(n). \tag{18}$$

Here $v_t^{(\mathrm{ideal})}$ is given by equation (15) and $v_t^{(\mathrm{exp})}$ is obtained from time-of-flight measurements using magnetic field sensors positioned along the tube. This separation clearly distinguishes the first-principles model from empirical corrections and avoids over parameterization.

Figure 5 shows the theoretical functions $v_t(n)$ obtained by equation (17) which are plotted for sets D15d1-D15d8. The velocity function exhibited by these graphs very well mirrors the real values of the terminal velocities observed in experimental measurements within Al/Cu tubes presented in figure 6.

In the terminal-velocity experiments, several aluminium (A–D) and copper (E–H) tubes of different diameters were used. For clarity, these tubes were labelled A–H and characterized by their inner radius, outer radius, wall thickness (in mm), and length in m): A (7.7, 10, 2.3, 0.75), B (8.8, 10, 1.2, 1), C (6.9, 8, 1.1, 1), D (4.9, 6, 1.1, 1), E (6.5, 7.5, 1, 1), F (8, 9, 1, 1), G (10, 11, 1, 1) and H (12.5, 14, 1.5, 1). This set of tubes enabled a systematic investigation of the influence of tube geometry and material on magnetic braking. As an example, the data shown in figure 6 were obtained using tube C.

7. Discussion

The present analysis shows that the magnetic induction at the front face of a magnet stack can be described in two complementary ways. The exact magnetostatic model leads to a compact closed-form expression obtained via a telescoping sum of individual contributions. Over finite ranges of stack height, the resulting discrete values exhibit an exponential saturation behaviour that can be conveniently represented using a geometric-series model.

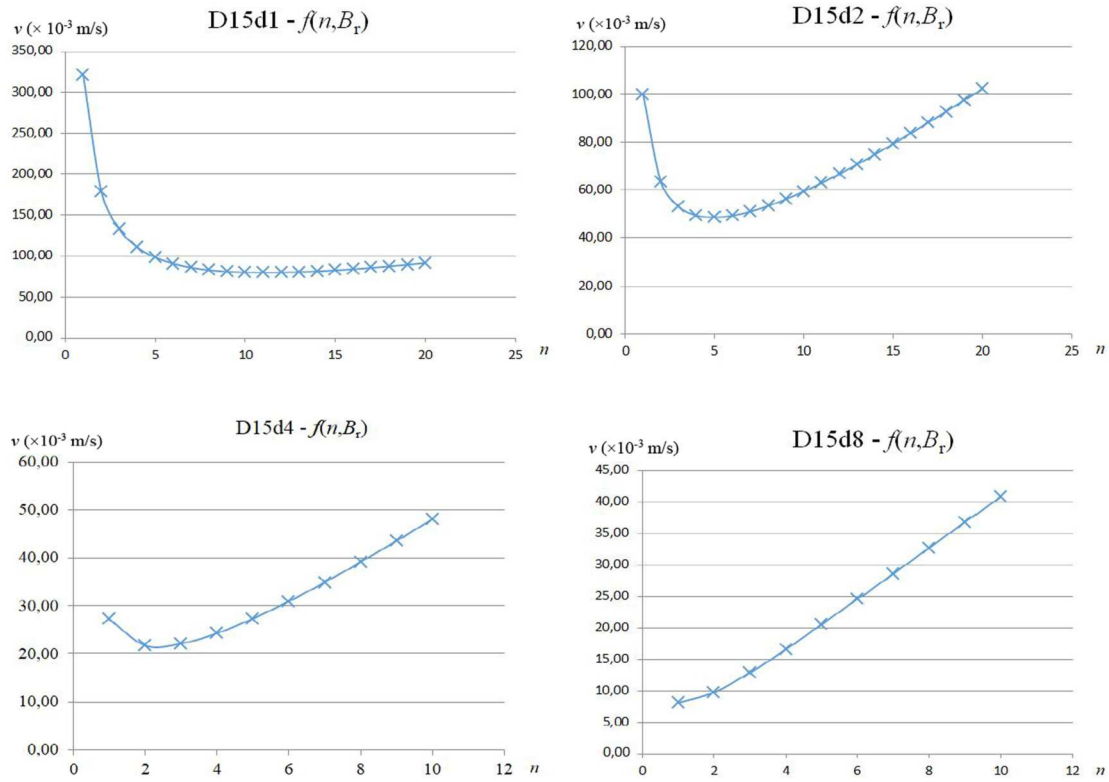

Figure 5. Function $v_t(n)$ obtained by equation (17) for set D15d1-d8.

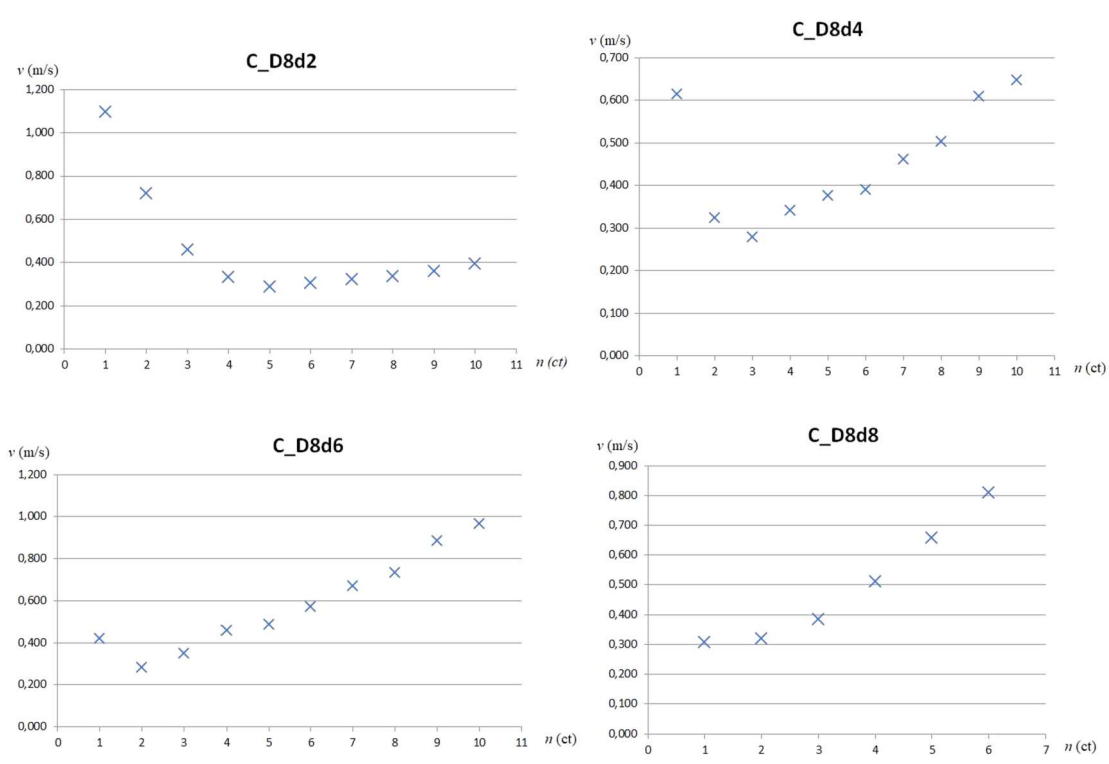

Figure 6. The experimental terminal velocities for a set of magnets ranging from D8d2 to D8d8.

It is important to emphasise that the geometric-series representation is an approximation rather than a fundamental property of the magnetic field. Its usefulness lies primarily in its simplicity and pedagogical transparency.

The observed exponential dependence of the effective saturation parameter on the aspect ratio d/D suggests that magnet geometry plays a dominant role in determining how rapidly the front-face field approaches its limiting value.

The field model also provides qualitative insight into the dependence of terminal velocity on stack height. Since the magnetic braking force scales approximately with B_r^2, the saturation of the radial component naturally explains the existence of a minimum in the velocity curve for short stacks.

The present model does not include demagnetization interactions between adjacent magnets or detailed boundary-value solutions for the conducting tube. These effects may introduce corrections at the few-percent level but do not alter the qualitative saturation behavior demonstrated here. Demagnetization corrections (e.g. [1]) may modify the effective B_{rem} inferred from near-field measurements; however, the saturation trend with n and the telescoping structure of equation (8) remain unaffected within the experimental accuracy reported here.

The telescoping structure of the exact expression (8) makes the saturation behaviour mathematically transparent, since each additional magnet contributes a progressively smaller correction term following an inverse-power decay.

8. Conclusion

We have presented a combined theoretical and experimental study of the magnetic field of cylindrical stacks of neodymium magnets. The front-face magnetic induction was derived from the standard axial field expression and expressed as a telescoping sum of individual magnet contributions.

Although the exact dependence on stack height follows a rational saturation law, the discrete experimental values can, over finite ranges, be accurately approximated by an exponential (geometric-series) model. The relative deviation between the exact magnetostatic expression and the exponential approximation remains within experimental uncertainty for the geometries investigated.

The novelty of the present treatment lies not in deriving a new magnetostatic formula for a single cylinder, but in revealing the telescoping structure of stacked contributions and in demonstrating that the resulting discrete sequence admits a simple exponential representation over experimentally relevant ranges.

The approach clarifies the physical origin of the saturation behaviour and provides a simple framework for interpreting the dependence of terminal velocity on stack length. Owing to its analytical transparency and experimental accessibility, the model is well suited for undergraduate instruction and advanced secondary-school laboratory work.

Data availability statement

All data that support the findings of this study are included within the article (and any supplementary files).

References

[1] Song W and Shuai C 2025 *J. Phys. Conf. Ser.* **3119** 012031
[2] Martín-Luna P *et al* 2024 *Eur. J. Phys.* **45** 065203
[3] Cava A E, Marin M B and Deaconu E M 2023 *2023 17th Int. Conf. on Engineering of Modern Electric Systems (EMES)* pp 1–4
[4] Zhang Y, Jiang M, Jia Y, Li X, Li Z and Wang H 2024 *Processes* **12** 2168
[5] Adams M P 2024 *Am. J. Phys.* **92** 576–82
[6] Shulman M D 2023 *J. Magn.* **28** 64–71
[7] Erofeenko V T 2020 *Informatics* **17** 103–19
[8] MacLatchy C S, Backman D and Sanford R A 1993 *Am. J. Phys.* **61** 1096–101
[9] Levin Y *et al* 2006 *Am. J. Phys.* **74** 815–7
[10] Roy M K 2007 *Am. J. Phys.* **75** 728–30
[11] Íñiguez J and Raposo V 2009 *Eur. J. Phys.* **30** L19–21
[12] Ireson G and Twidle J 2008 *Eur. J. Phys.* **29** 745–51
[13] Donoso G *et al* 2011 *Am. J. Phys.* **79** 193–200
[14] Maryam S, Rezaei B and Kowsary F 2014 *Phys. Educ.* **49** 319
[15] Pal S K *et al* 2024 *Phys. Educ.* **59** 015022
[16] Camacho J and Sosa V 2013 *Rev. Mex. Fís. E* **59** 8–17 available online at (https://www.scielo.org.mx/pdf/rmfe/v59n1/v59n1a2.pdf)
[17] Connors M 2002 *Phys. Teach.* **40** 308–11
[18] Médjahdi K 2021 *Eur. J. Phys.* **42** 055804
[19] Griffiths D J 2017 *Introduction to Electrodynamics* 4th edn (Cambridge University Press)
[20] Kodejška Č 2025 (https://www.fyzikar.cz/EDS/Nd-magnets-induction-terminal-velocity.zip)